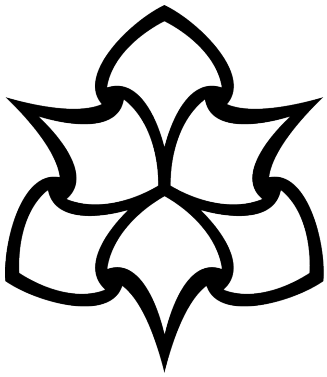

Investigating the Integrity of Graphene towards the Electrochemical Oxygen Evolution Reaction (OER)

Alejandro García-Miranda Ferrari [a,b], Dr. Dale A. C. Brownson [a,b], and Prof. Craig E. Banks [a,b*]

[a]: *Faculty of Science and Engineering, Manchester Metropolitan University, Chester Street, Manchester M1 5GD, UK*

[b]: *Manchester Fuel Cell Innovation Centre, Manchester Metropolitan University, Chester Street, Manchester M1 5GD, UK*

*To whom correspondence should be addressed
Email: c.banks@mmu.ac.uk; Tel: ++(0)1612471196; Fax: ++(0)1612476831
Website: www.craigbanksresearch.com

Keywords: Graphene, Electrochemistry, Raman Spectroscopy, Oxygen Evolution Reaction (OER), 2D Materials

Abstract: Mono-, few- and multi- layer graphene is explored towards the electrochemical Oxygen Evolution Reaction (OER). Raman mapping characterisation is performed, revealing that the structure of basal plane graphene is damaged due to the electrochemical perturbation of the OER. Electrochemical perturbation, in the form of electrochemical potential scanning (linear sweep voltammetry), and a thorough comparison of the OER at different scan rates and chronoamperometry tests at different voltages, create active edge plane sites/defects upon the basal plane graphene surface in the case of the mono- and few- layer graphene electrodes. The electrochemical performance gradually decreases with consecutive OER scans upon a given graphene electrode, with the process damaging the basal plane graphene sheet, after which there is a loss in the electrochemical signal due to a loss in electrically conductive pathways. Importantly, the severity of these changes is dependent on the potential and chosen scan rate that is applied to the graphene electrode. In contrast, however, multilayer graphene's initial performance towards the OER process improves after the first few scans, which is likely due to an increase in the coverage of edge plane sites/defects and its underlying layers maintaining electrical contact. This work indicates the importance of the scan rate and potential limits applied to graphene electrodes in addition to the relationship between the number of layers and structural integrity. This new knowledge is of fundamental importance to be advantageously applied within the energy sector and beyond.

1. Introduction

Water oxidation, namely the oxygen evolution reaction (OER), is part of the water splitting reaction and involves a complex process with a solid catalyst, electrolyte, and both gas-/liquid-phase reactants and products[1]. The OER is recognized as a very sluggish reaction in water electrolysis for clean hydrogen energy, due to not being kinetically favoured and usually requires precious iridium- or ruthenium-based catalysts to reduce the electrochemical overpotential[2]. Water splitting consists of the reaction of water molecules to form molecular hydrogen and molecular oxygen, usually described as two half reactions: at the cathode, protons are reduced to hydrogen (hydrogen evolution reaction; HER); and at the anode, water is oxidized to oxygen (oxygen evolution reaction; OER). The OER involves four proton-coupled electron transfers and oxygen-oxygen bond formation in *acidic* conditions: $2H_2O \rightarrow O_2 + 4H^+ + 4e^-$. In *alkaline* conditions the OER involves four hydroxyl groups (OH^-) being transformed into H_2O and O_2 molecules with four electrons involved $4OH^- \rightarrow O_2 + 2H_2O + 4e^-$.

Currently, there is significant research interest into studying the fundamentals of the OER in order to obtain more active catalysts[3]. At the same time, the key to developing mass-producible and economical fuel cells is realizing the use of nonprecious metals as highly active catalysts[4]. Although carbon itself has been reported slow/less competitive for the HER/OER reactions[5], recently carbon-based substrates have been reported to be a viable source for durable and affordable OER catalysts due to their high conductivity and large surface area[5a, 6]. A promising alternative is the combination of carbon-nitrogen with the high activity of earth-abundant transition metals (such as Co, Ni, Mn, Fe *etc*.)[7]. It is also important to consider that thick carbon shells have been reported to obstruct the electron transfer from metals to carbon, reducing the catalytic activity of the catalyst[8]. As a result, there is interest in developing graphene-based catalysts using innovative strategies including surface functionalization[9], geometric arranging[10] and heteroatom doping[11]. It is important to add the lack of studies regarding pristine 2D graphene (CVD) application, large-quantity synthesis and integration for

energy applications[12], and the effect of the graphene's edge structures because of the high complexity of coexisting edge configurations[5b]. Therefore, there is a need to fundamentally understand the intrinsic relationship of the bare graphene structures (mono, few, multi) correlated to electrochemical performance for the future application of CVD graphene-based catalysts.

Herein, we explore and fully characterize the electrochemical stability of mono-, few- and multi-layer Chemical Vapour Deposition (CVD) grown graphene electrodes towards the OER, with the purpose of understanding the difference of graphene structure and electrochemical relationship using the OER as an important electrochemical process, which has significant importance upon the design of future graphene-based OER catalysts.

2. Results and discussion

Attention was first turned to benchmarking mono-, few- and multi-layer (basal plane) graphene as an electrode platform towards the OER within alkaline media (0.1 M KOH), as is common within the literature[13]. **Figure 1** shows electrochemical scanning stability experiments using mono-, few- and multi-layer graphene electrodes/surfaces towards the OER after five OER linear sweep voltammetry (LSV) scans (from 0.21 to +1.61 V(*vs.* RHE); Scan rate: 25 mV s^{-1}). As one can see in Figure 1A, the electrochemical performance of mono-layer graphene towards the OER decays when successive scans are completed; note also that the electrochemical signal of the first scan is highly likely perturbed by bubbles being formed upon the graphene electrode's surface, which are oxygen bubbles being formed as a result of the OER occurring at edge plane sites/defects upon the basal plane graphene surface. The origin of electron transfer properties pristine graphene has been recently confirmed to happen at the edges[14]. and in particular for the OER application, zigzag edge configurations give better performance than armchair motifs, playing both a positive role in the OER[5b].

Note that full physicochemical characterization of the various graphene samples utilized within this work have been previously reported[15], showing that the Raman spectra of the monolayer graphene sheets reveals that the full width at half-maximum (FWHM) of the 2D band corresponds to 34.72 cm^{-1}, which suggests the presence of mono-layer graphene[3-4]; also the ratio of the intensity of the G/2D bands is 0.72, confirming that the graphene samples are indeed made of a single layer of graphene. The Raman spectrum of the few- and multi-layer films reveals an intensity ratio of G/2D of 1.00 and 1.76 respectively, confirming again that they are, as name, made of few- and multi-layer graphene respectively. 1.76 suggesting that such electrode is comprised of multilayer graphene.

The first OER scan using the mono-layer graphene has a current of 3.13 μA cm^{-2} (at +1.41 V(*vs.* RHE)) after which there is a significant decrease to 2.24, 1.78, 1.58 and 0.29 μA cm^{-2} for the successive five scans respectively, indicating a decay in the electrochemical

current and reduced electrochemical activity. These changing electrochemical observations clearly suggest a physical change/damage of the mono-layer basal plane graphene electrode and in the conductive (electron) pathways. In the case of multi-layer graphene, as shown in Figure 1B, the current increases when further scans are performed from 108 μA cm^{-2} to 3234 μA cm^{-2} (at +1.4 V(*vs.* RHE)) at the fifth scan, having a similar LSV profile and values between the 30^{th} and 50^{th} consecutive scans, where the electrochemical performance stabilizes; this is likely to be due to the activation of the electrode and/or creation of new edge plane sites/defects. Finally, the electrochemical response of few-layer graphene towards the OER, as depicted in Figure 1C, shows a gradual decrease in the electrochemical performance during 5 individual LSV scans (from 11.3 μA cm^{-2} at the first scan down to 0.85 μA cm^{-2} (at +1.61 V (*vs.* RHE)) at the fifth scan), similar to the case observed with mono-layer graphene, demonstrating that a reduced amount of graphene layers stacked (mono- or few-layer graphene) decrease their electrochemical response when scanning multiple LSV towards the OER. Based on this, Raman mapping characterisation is performed in order to elucidate if the number of layers affects the integrity of the graphene sheet when utilised in electrochemistry.

In **Figure 2** the Raman mapping characterisation and optical images from the graphene samples/electrodes presented in Figure 1 can be observed. It is clear that the mono- and few-layer basal plane graphene surfaces are mostly damaged and show the lack of characteristic Raman peaks, which usually occur at *ca*. 1590 cm^{-1} and 2690 cm^{-1} respectively, and are widely used to quantify the number of graphene layers[16] (see Experimental Information for further data); such peaks *are* evident *prior* to experimental probing[17] with 5 LSV scans. Conversely, the multi-layer graphene electrode remains mostly unaltered and constant across its surface throughout experiments, evidenced by to the optical and Raman mapping characterisation (showing an inherent resistance to such surface changes). These results confirm the importance of the number of layers present in CVD Graphene. The existence of several graphene layers stacked are beneficial, in this case, in terms of maintaining the structural integrity of the

graphene film (when the exposed top graphene layer fails/breaks, the several underlying graphene layers will become the top one successively acting as a renewal mechanism). In the case of mono- and few-layer graphene, where there is only 1 or few layers present, once the first layer(s) is/are compromised, the electrode will eventually fail with consecutive LSV OER scans. It is important to note that herein we focus on the damage of graphene, because it has been previously reported its impermeability to all gases and liquids[18], therefore the underlying SiO_2 substrate is not in contact with the solution prior to any damage in the electrode.

Attention was then turned to considering how the different scan rates applied to the electrode surface can affect the structural integrity of the mono-layer graphene. Note that this is a common approach to characterise the electrochemical performance of an electrode material (voltammetric scan rate study) to determine heterogeneous electron transfer kinetics, providing an electrochemical benchmarking of the graphene (electrode) surface under investigation. **Figure 3** shows the optical images and Raman maps of both 'unused' and 'used' (following 5 LSV OER scans) electrodes, after being used at different scan rates (2.5, 25, 250 and 2500 mV s^{-1}). The damage created on the graphene surfaces is evident, the degree of damage is related to the scan rate applied. It is clear that faster scan rates create extended damage on the surface of the electrode, having a more focused or confined damage pattern than when slower scan rates are applied. Interestingly, similar microstructural and compositional surface fragmentation have been previously reported in graphite electrodes, due to prolonged and variable scan rates potential cycling when exploring Li-ion storage applications[19]. This could suggest, in our view, that *in-situ* generated gas bubbles and Li-ion intercalation move along the surface of graphitic films creating similar damage/defects to the surface of the electrode. The rate of the voltage step applied has been described before as one factor that has a role in graphite electrode degradation, added to the role that it plays making a more kinetically favourable reaction as explained in the answer above. When faster scan rates are applied, the newly generated species are generated faster (than when slower scan rates are applied), not allowing

the electrode (very thin in this case, as a one single layer of carbon atoms) to accommodate the charge and current passing through it), and the generated bubbles have a faster growing rate which translates in more aggressive/faster movements across the surface and sharper/more sudden growth, detachment and departure from the surface.

Next, chronoamperometry (CA) was utilised in order to analyse the origin of the breakup of graphene's structure when applied towards the OER. Herein, we hold a fixed potential for 280 seconds, which corresponds to the same amount of time as the electrode used in the scanning stability studies at 25 mV s^{-1} (Figures 1 and 2). In **Figure 4**, CA studies are performed at +0.61, +1.01, +1.41 and +1.61 V (*vs.* RHE) for samples named 1 to 4 of mono-layer graphene respectively, showing optical images, Raman profiles and Raman mapping characterisation for each sample 'before' and 'after' applying the fixed potential. Sample 1 and 2 (Figure 4A to F and G to L respectively) have the typical Raman peaks in their profiles both before and after being used; although some localized damage can be seen. Sample 3 (Figure 4M to 4R) shows the presence of a continuous graphene sheet after being used for 280 seconds at 1.41 V (*vs.* RHE), however, upon inspection of the Raman profile one can observe the presence of a graphene D band (*ca*. 1350 cm^{-1}) that corresponds to defects in the lattice structure; similar to that observed in graphene quantum dots[20] (QDT: sometimes also called nanographene[21]) or ozonolyzed CVD graphene[22]. Sample 4 (Figure 4S to X) shows a large damaged area after holding 1.61 V (*vs.* RHE) for 280 seconds, in addition to the presence of the characteristic D band/peak (*ca*. 1350 cm^{-1}) previously described in Sample 3.

As shown above, clearly, an important factor to consider in terms of material integrity in the OER in the degradation of the graphene sheet is the physical movement of the generated oxygen bubbles themselves, which are generated at edge plane sites/defects. Electrochemical systems have been reported to suffer poor management of evolving gas bubbles[23]. Gas formation can be divided in four stages that occur simultaneously on the surface of the electrode: nucleation, growth, detachment and rise[24]. In order to capture the graphene damage

due to O_2 evolution, as a result of the OER occurring at the various graphene electrodes/surfaces, as it takes place, an *in-situ* images were captured, showing a mono-layer graphene electrode while CA was applied (at +1.61 V (*vs.* RHE)) . **Figure 5** depicts captures taken, showing the graphene surface and the nucleation, growth and detachment of O_2 at ten, twenty, thirty and forty seconds (Figure 5 A, B, C and D respectively) since the fixed potential is applied. One can see the direct damage created to the surface of the mono-layer graphene when a bubble is nucleating, growing and coalescing with other bubbles and while moving across the electrode. Large bubbles act as collectors, attracting smaller growing bubbles, inducing mechanical forces, heat transfer and mass diffusion due to supersaturation of surrounding liquid solution[25] and are likely the reason of the collapse of the graphene integrity. **Figure 6** presents a schematic overview of the proposed mechanism of degradation of the mono and few-layer graphene (electrode) surface, which shows that the detachment or departure of bubbles from the electrode surface can also cause damage to the electrode. Once a bubble grows, fuelled at edge plane sites/defects via the OER reaction, that is large enough to reach a critical volume, at which the flotation force surpasses the interfacial tension between the oxygen filled gas bubble and the electrode surface, the bubble will detach or collapse from the surface of the electrode into the bulk solution. The collapse of the bubble can lead to surface cleaning, via frictional forces as it is "filled" at active edge plane sites/defects or in addition, surface cavitation/bubble collapse, ablation and/or fracture[26]. We infer that this is the mechanism that results in the degradation of graphene surfaces, rather than graphene not being able to support such large over-potentials. It is likely that the mechanism for breakup of the graphene sheet occurs due to three contributing factors: i) given that the graphene structure is too thin/fragile on the macro-scale, it cannot accommodate the charge/current passed through it, although there are some reports indicating Graphene's breakdown current density in air to be as high of ~10^8 A cm^{-2} [27], however we have not seen any reports of macroscale graphene samples within electrolytes; ii) bubbles are formed on the surface of the graphene sheet and break it *via*

frictional forces and when the bubbles collapse (as described above); and iii) bubbles evolve/form from underneath the graphene sheet (which is unlikely). Currently, there is no way to de-convolute the degradation process from that of bubble generation/surface motion from that of charge instability, but we inferred the former based upon observations (Figure 5) and note that the predominant mechanism is likely that of (ii) the bubbles formed upon the graphene surface and the resultant physical forces induced.

The data presented herein has shown the damage sustained to a graphene structure when applied as an electrode material towards the OER. This damage is directly dependent on the number of layers comprising the graphene electrode, the applied voltage (voltages higher than +1.41 V(*vs.* RHE) in this case) and scan rate applied (faster scan rates create more extensive damage). This behaviour indicates that the generation and movement of O_2 bubbles results in the graphene surface first becoming defective (according to the presence of a D band in its Raman profile) and later collapsing/breaking-up completely. Note that it has been reported previously that mono- and few-layer CVD graphene is not a beneficial electrode material towards the HER due to the generation of H_2 bubbles[15]; although at first its response improves the electrochemical reversibility of the reaction due to an increase in the edge-site/defect coverage prior to electrochemical cycling damaging the electric pathway. In the case of this work, the application of CVD graphene towards the OER induces the creation of defects on/across the electrode's surface, likely due to the generation and movement of O_2 bubbles, creating rips, holes and defect-dense graphene domains akin to nano-ribbon like structures, which finally disrupt the conductive pathway, ultimately resulting in a loss of electrochemical signal.

3. Conclusion

The behaviour described in this manuscript shows, for the first time, that mono- and few-layer CVD graphene electrodes break-up when utilised towards the OER. The mechanism in

which the graphene structure rips occurs when potentials more positive than +1.41 V (*vs.* RHE) are reached. Evidence of small fragments of graphene/ nano-ribbon like structures was found, according to the Raman characterisation, when a potential of 1.41 V (*vs.* RHE) is held for prolonged time. More positive potentials fixed for the same period of time (as per cycling potential exposure times) created extended damage on the mono-layer graphene sheet. The scan rate applied to the electrode surface was also shown to have an effect on the stability of the reaction, creating more damage when faster scan rates are applied. This reported response (or instability) is evident at both CVD mono- and few-layer graphene electrodes; what is important however, is that multi-layer graphene *does not* present the same inherent limitations, with this material remaining stable after OER scanning for a larger number of consecutive scans. These findings are relevant to those working with CVD graphene at high potentials; given that the integrity of the material's structure is compromised, it is evident that CVD mono- and few-layer graphene are *not* suitable electrode materials towards the OER. Such work is of fundamental importance when graphene surfaces are used either "as is" or as the basis of catalysts as used in the OER.

4. Experimental Section

Experimental Details:

All chemicals used were of analytical grade and were used as received from the supplier (Sigma-Aldrich, Irvine, UK) without any further purification. All solutions were prepared with deionized water of resistivity no less than 18.2 MΩ cm and were vigorously degassed prior to electrochemical measurements with high purity, oxygen free nitrogen. The tested solutions were 0.1 M KOH.

Electrochemical measurements were performed using a three-electrode system on an Autolab PGSTAT204 potentiostat (Metrohm Autolab, Utrecht, The Netherlands). Working electrodes were: commercially obtained Chemical Vapor Deposition (CVD) synthesized mono-layer, a few-layer (*quasi*-graphene) and multilayer-graphene films supported on an oxidized silicon wafer. A Pt wire counter/auxiliary electrode and a silver/silver chloride (saturated Ag/AgCl; converted to *vs*. RHE as +0.210V *vs.* RHE) reference electrode completed the circuit. Graphene working electrodes were secured into a 3D printed electrochemical cell, as described by our research group in previous work[14].

The commercially available CVD grown graphene films, that have been used in our previous work[15, 28], were obtained from 'Graphene Supermarket' (Reading, MA, USA) and are known as 'graphene on 285 nm SiO_2 Wafer' and have been previously reported and characterized in the literature[15, 28b, 29]; the exact details are proprietary information[29b, 29c, 30].

Raman Mapping Spectroscopy data was performed using XploRA PLUS (Horiba, UK) fitted with a 638 nm excitation laser at a power of 3 mW to avoid any heating effects. Spectra were recorded using a 5 seconds exposure time for 1 accumulations at each point. To collect the map a step size of 40×40 μm and a Raman profile between the region of 1300 and 3200 cm^{-1} was employed, mapping a circular-shaped area of 2.6 mm of diameter. 3D Raman map figures depict the intensity of the characteristic Raman G band for graphene (*ca*. 1590 cm^{-1}) recorded from their full Raman spectra. Graphene's Raman G band is related to the first-order Raman

band of all sp^2 hybridized carbons[17, 31]. Graphene's 2D Raman band is always present and originates from a resonant process, depending its band position on the laser excitation[32].

Acknowledgements

Funding from the Engineering and Physical Sciences Research Council (Reference: EP/N001877/1) is acknowledged.

Author contributions:

C.E.B conceived the idea. A.G.M.F, C.E.B and D.A.C.B designed the experiments. A.G.M.F performed the experiments. A.G.M.F, D.A.C.B and C.E.B performed the data analysis. All authors wrote the manuscript, discussed the results and are agreed on the final version. C.E.B coordinated the overall project.

Received: ((will be filled in by the editorial staff))
Revised: ((will be filled in by the editorial staff))
Published online: ((will be filled in by the editorial staff))

5. References

[1] aM. Ding, Q. He, G. Wang, H.-C. Cheng, Y. Huang, X. Duan, Nat. Commun. **2015**, 6, 7867; bP. Wang, M. Yan, J. Meng, G. Jiang, L. Qu, X. Pan, J. Z. Liu, L. Mai, Nature Communications **2017**, 8, 645.

[2] Y. Jiao, Y. Zheng, M. Jaroniec, S. Z. Qiao, Chem. Soc. Rev. **2015**, 44, 2060-2086.

[3] aS. Trasatti, Electrochim. Acta **1984**, 29, 1503-1512; bY. Matsumoto, E. Sato, Mater. Chem. Phys. **1986**, 14, 397-426; cJ. Rossmeisl, Z. W. Qu, H. Zhu, G. J. Kroes, J. K. Nørskov, J. Electroanal. Chem. **2007**, 607, 83-89; dI. C. Man, H.-Y. Su, F. Calle-Vallejo, H. A. Hansen, J. I. Martínez, N. G. Inoglu, J. Kitchin, T. F. Jaramillo, J. K. Nørskov, J. Rossmeisl, ChemCatChem **2011**, 3, 1159-1165; eC. C. L. McCrory, S. Jung, I. M. Ferrer, S. M. Chatman, J. C. Peters, T. F. Jaramillo, J. Am. Chem. Soc. **2015**, 137, 4347-4357.

[4] aL. C. Seitz, T. J. P. Hersbach, D. Nordlund, T. F. Jaramillo, J. Phys. Chem. Lett. **2015**, 6, 4178-4183; bJ. Chang, Q. Lv, G. Li, J. Ge, C. Liu, W. Xing, Appl. Catal., B, Vol. 204, **2016**; cG. Wu, A. Santandreu, W. Kellogg, S. Gupta, O. Ogoke, H. Zhang, H.-L. Wang, L. Dai, Nano Energy **2016**, 29, 83-110; dD. Chen, C. Chen, Z. M. Baiyee, Z. Shao, F. Ciucci, Chem. Rev. **2015**, 115, 9869-9921; eJ. Zhang, Z. Zhao, Z. Xia, L. Dai, Nat. Nanotechnol. **2015**, 10, 444.

[5] aL. Zhang, J. Xiao, H. Wang, M. Shao, ACS Catal. **2017**, 7, 7855-7865; bY. Lin, Q. Lu, F. Song, L. Yu, A. K. Mechler, R. Schlögl, S. Heumann, Angew. Chem., Int. Ed. Engl. **2019**, 58, 8917-8921.

[6] aY. Mu, H. Liang, J. Hu, L. Jiang, L. Wan, The Journal of Physical Chemistry B 2005, 109, 22212-22216; bY. Liang, H. Wang, J. Zhou, Y. Li, J. Wang, T. Regier, H. Dai, J. Am. Chem. Soc. **2012**, 134, 3517-3523; cX. Bian, J. Zhu, L. Liao, M. D. Scanlon, P. Ge, C. Ji, H. H. Girault, B. Liu, Electrochem. Commun. **2012**, 22, 128-132; dQ. Liu, J. Jin, J. Zhang, ACS Appl. Mater. Interfaces **2013**, 5, 5002-5008.

[7] aX. Li, P. Cui, W. Zhong, J. Li, X. Wang, Z. Wang, J. Jiang, Chem. Commun. **2016**, 52, 13233-13236; bF. Calle-Vallejo, J. Tymoczko, V. Colic, Q. H. Vu, M. D. Pohl, K. Morgenstern, D. Loffreda, P. Sautet, W. Schuhmann, A. S. Bandarenka, Science **2015**, 350, 185-189; cK. Ding, A. Gulec, A. M. Johnson, N. M. Schweitzer, G. D. Stucky, L. D. Marks, P. C. Stair, Science **2015**, 350, 189-192; dG. Gao, Y. Jiao, E. R. Waclawik, A. Du, J. Am. Chem. Soc. **2016**, 138, 6292-6297; eX. Li, W. Zhong, P. Cui, J. Li, J. Jiang, J. Phys. Chem. Lett. **2016**, 7, 1750-1755.

[8] aJ. Deng, L. Yu, D. Deng, X. Chen, F. Yang, X. Bao, J. Mater. Chem. A **2013**, 1, 14868-14873; bJ. Deng, P. Ren, D. Deng, L. Yu, F. Yang, X. Bao, Energy Environ. Sci. **2014**, 7, 1919-1923.

[9] V. S. Sapner, B. B. Mulik, Renuka V. Digraskar, S. S. Narwade, B. R. Sathe, RSC Adv. **2019**, 9, 6444-6451.

[10] T. Y. Ma, S. Dai, M. Jaroniec, S. Z. Qiao, Angew Chem Int Ed Engl **2014**, 53, 7281-7285.

[11] J. P. Paraknowitsch, A. Thomas, Energy Environ. Sci. **2013**, 6, 2839-2855.

[12] Z. Chen, W. Ren, L. Gao, B. Liu, S. Pei, H.-M. Cheng, Nat. Mater. **2011**, 10, 424.

[13] C. C. L. McCrory, S. Jung, J. C. Peters, T. F. Jaramillo, J. Am. Chem. Soc. **2013**, 135, 16977-16987.

[14] A. Garcia-Miranda Ferrari, C. W. Foster, D. A. C. Brownson, K. A. Whitehead, C. E. Banks, Sci Rep **2019**, 9, 12814.

[15] A. García-Miranda Ferrari, D. A. C. Brownson, C. E. Banks, Sci. Rep. **2019**, Under review.

[16] A. C. Ferrari, J. C. Meyer, V. Scardaci, C. Casiraghi, M. Lazzeri, F. Mauri, S. Piscanec, D. Jiang, K. S. Novoselov, S. Roth, A. K. Geim, Phys. Rev. Lett. **2006**, 97, 187401.

[17] A. C. Ferrari, Solid State Commun. **2007**, 143, 47-57.
[18] aV. Berry, Carbon $V 62 **2013**, 1-10; bR. K. Singh Raman, P. Chakraborty Banerjee, D. E. Lobo, H. Gullapalli, M. Sumandasa, A. Kumar, L. Choudhary, R. Tkacz, P. M. Ajayan, M. Majumder, Carbon **2012**, 50, 4040-4045.
[19] aS. Bhattacharya, A. R. Riahi, A. T. Alpas, MRS Proceedings **2012**, 1388, mrsf11-1388-f1312-1311; bS. Bhattacharya, A. T. Alpas, Carbon **2012**, 50, 5359-5371; cE. Markervich, G. Salitra, M. D. Levi, D. Aurbach, J. Power Sources **2005**, 146, 146-150.
[20] aD. B. Shinde, V. K. Pillai, Chem. - Eur. J. **2012**, 18, 12522-12528; bH. Cheng, Y. Zhao, Y. Fan, X. Xie, L. Qu, G. Shi, ACS Nano **2012**, 6, 2237-2244; cJ. Lee, K. Kim, W. I. Park, B.-H. Kim, J. H. Park, T.-H. Kim, S. Bong, C.-H. Kim, G. Chae, M. Jun, Y. Hwang, Y. S. Jung, S. Jeon, Nano Lett. **2012**, 12, 6078-6083; dL. Fan, M. Zhu, X. Lee, R. Zhang, K. Wang, J. Wei, M. Zhong, D. Wu, H. Zhu, Part. Part. Syst. Charact. **2013**, 30, 764-769.
[21] J.-B. Wu, M.-L. Lin, X. Cong, H.-N. Liu, P.-H. Tan, Chem. Soc. Rev. **2018**, 47, 1822-1873.
[22] M. Bodik, A. Zahoranova, M. Micusik, N. Bugarova, Z. Spitalsky, M. Omastova, E. Majkova, M. Jergel, P. Siffalovic, Nanotechnology **2017**, 28, 145601.
[23] A. Taqieddin, R. Nazari, L. Rajic, A. Alshawabkeh, J. Electrochem. Soc. **2017**, 164, E448-E459.
[24] aC. A. C. Sequeira, D. M. F. Santos, B. Šljukić, L. Amaral, Brazilian Journal of Physics 2013, 43, 199-208; bH. Vogt, K. Stephan, Electrochim. Acta **2015**, 155, 348-356.
[25] C. W. M. P. Sillen, Eindhoven **1983**.
[26] C. E. Banks, R. G. Compton, ChemPhysChem **2003**, 4, 169-178.
[27] C. Kang, S. Lee, Y. Lee, H. Hwang, C. Cho, S. K. Lim, J. Heo, H.-J. Chung, H. Yang, S. Seo, B. Lee, IEEE Electron Device Lett., IEEE **2011**, 32, 1591-1593.
[28] aD. A. C. Brownson, S. A. Varey, F. Hussain, S. J. Haigh, C. E. Banks, Nanoscale **2014**, 6, 1607-1621; bD. A. C. Brownson, C. E. Banks, Phys. Chem. Chem. Phys. **2012**, 14, 8264-8281; cD. A. C. Brownson, P. J. Kelly, C. E. Banks, RSC Adv. **2015**, 5, 37281-37286.
[29] aX. Li, W. Cai, J. An, S. Kim, J. Nah, D. Yang, R. Piner, A. Velamakanni, I. Jung, E. Tutuc, S. K. Banerjee, L. Colombo, R. S. Ruoff, Science **2009**, 324, 1312-1314; bX. Li, Y. Zhu, W. Cai, M. Borysiak, B. Han, D. Chen, R. D. Piner, L. Colombo, R. S. Ruoff, Nano Lett. **2009**, 9, 4359-4363; cX. Liang, B. A. Sperling, I. Calizo, G. Cheng, C. A. Hacker, Q. Zhang, Y. Obeng, K. Yan, H. Peng, Q. Li, X. Zhu, H. Yuan, A. R. Walker, Z. Liu, L. M. Peng, C. A. Richter, ACS Nano **2011**, 5, 9144-9153.
[30] X. Li, W. Cai, J. An, S. Kim, J. Nah, D. Yang, R. Piner, A. Velamakanni, I. Jung, E. Tutuc, S. K. Banerjee, L. Colombo, R. S. Ruoff, Science **2009**, 324, 1312-1314.
[31] aA. C. Ferrari, J. Robertson, Phys. Rev. B **2000**, 61, 14095-14107; bF. Tuinstra, J. L. Koenig, J. Chem. Phys. **1970**, 53, 1126-1130; cF. Negri, E. d. Donato, M. Tommasini, C. Castiglioni, G. Zerbi, K. Müllen, J. Chem. Phys. **2004**, 120, 11889-11900.
[32] aA. C. Ferrari, D. M. Basko, Nat. Nanotechnol. **2013**, 8, 235; bV. N. Popov, J. Phys. Conf. Ser. 2016, 682, 012013.

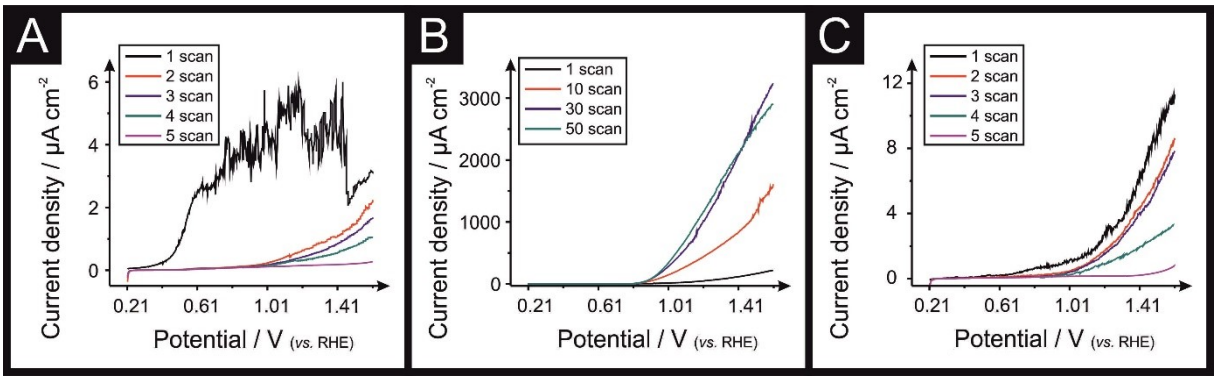

Figure 1. Scanning stability experiments of mono- (A), multi- (B) and few- (C) layer graphene electrodes using linear sweep voltammetry (LSV) towards the OER; Scan rate: 25 mV s^{-1}; *vs*. RHE; Solution: 0.1 M KOH. Note that the voltammetric scans are performed continuously.

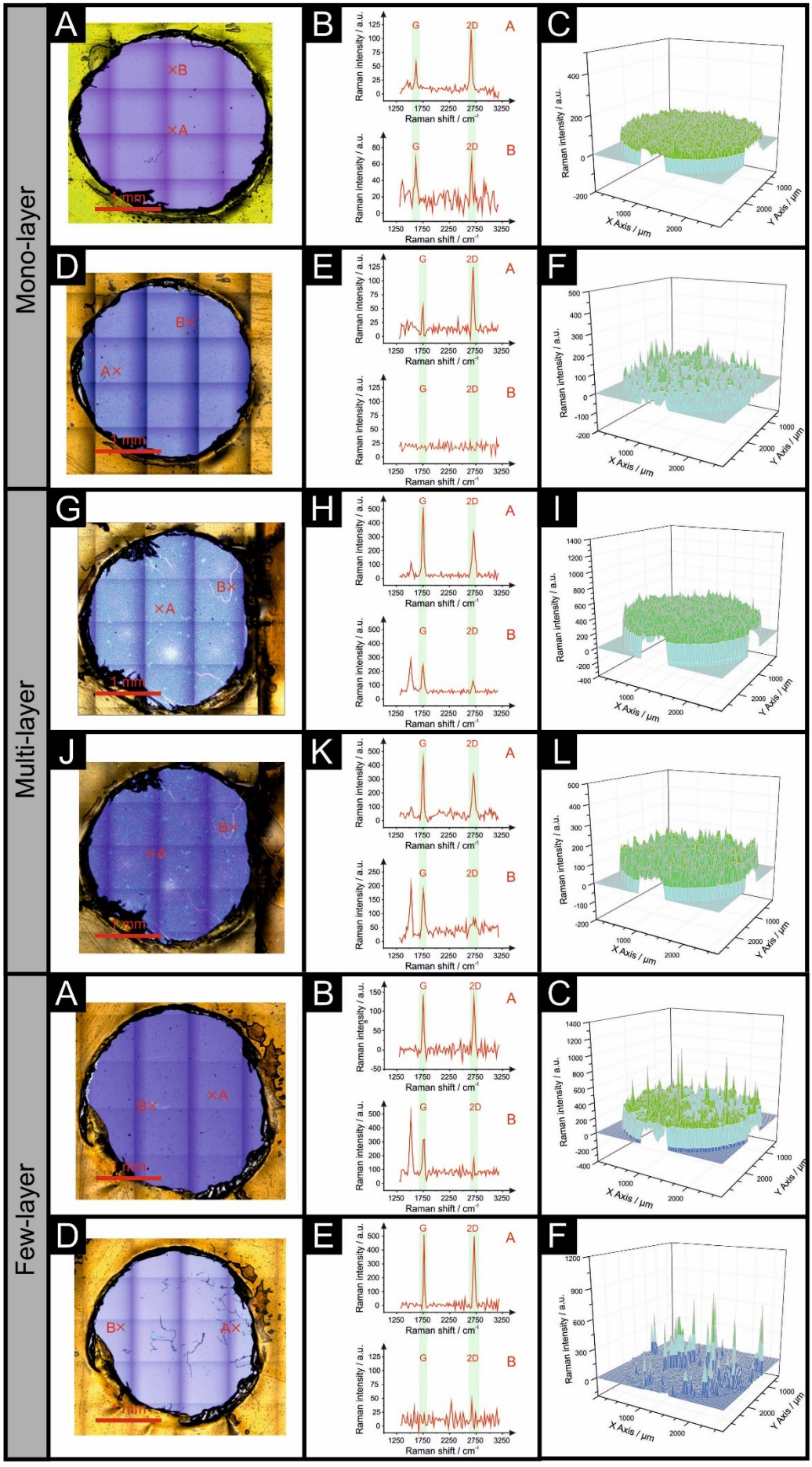
Mono-layer
Multi-layer
Few-layer
A
B
C
D
E
F
G
H
I
J
K
L
×B
×A
B×
A×
1 mm
G
2D
Raman intensity / a.u.
Raman shift / cm⁻¹
X Axis / μm
Y Axis / μm

Figure 2. Scanning stability experiments using mono-, few and multi-layer graphene; Mono-layer graphene (A to F) showing an optical image, its Raman profile and 3D Raman map (A, B and C respectively) of the unused mono-layer graphene. Mono-layer graphene after 5 LSV OER scans optical, its Raman profile and 3D Raman map (D to F respectively). Multi-layer graphene (G to L) showing an optical image, its Raman profile and 3D Raman map (G to I) of the unused multi-layer graphene. Multi-layer graphene after 50 LSV OER scans optical, its Raman profile and 3D Raman map (J to L). Few-layer graphene (M to R) showing an optical image, its Raman profile and 3D Raman map (M to O) of the unused few-layer graphene. Few-layer graphene after 5 LSV OER scans optical, its Raman profile and 3D Raman map (P to R). (Solution: 0.1 M KOH; *vs*. RHE). Raman maps show intensity of Graphene's G band (*ca*. 1590 cm^{-1}).

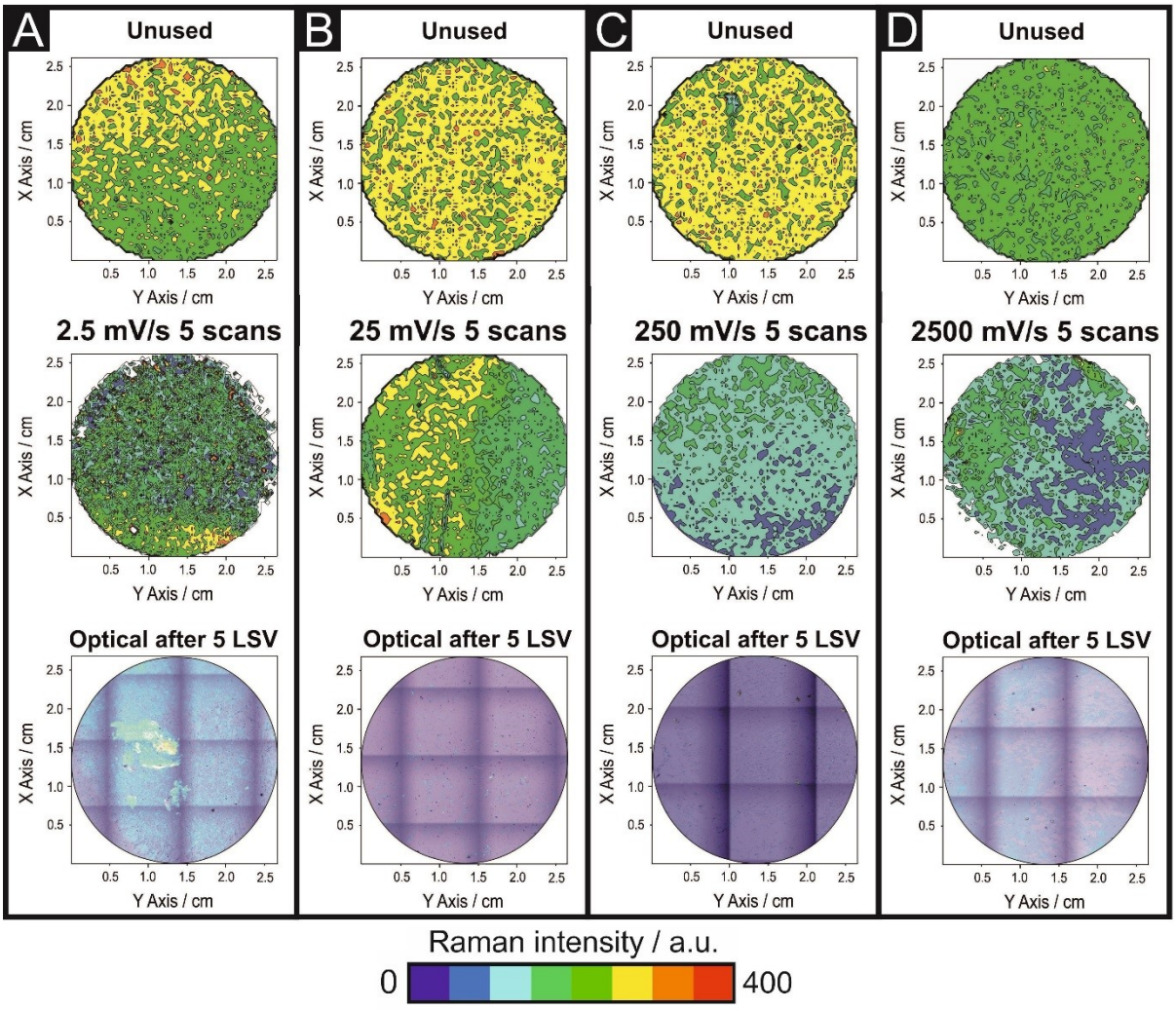

Figure 3. Scan rate stability experiments using mono-layer graphene at 2.5 (A), 25 (B), 250 (C) and 2500 (D) mV s^{-1}, showing the Raman mapping characterisation before and after 5 LSV OER scans and optical image of the electrode after the 5 LSV OER scans. (Solution: 0.1 M KOH; *vs*. RHE). Raman maps show intensity of Graphene's G band (*ca*. 1590 cm^{-1}).

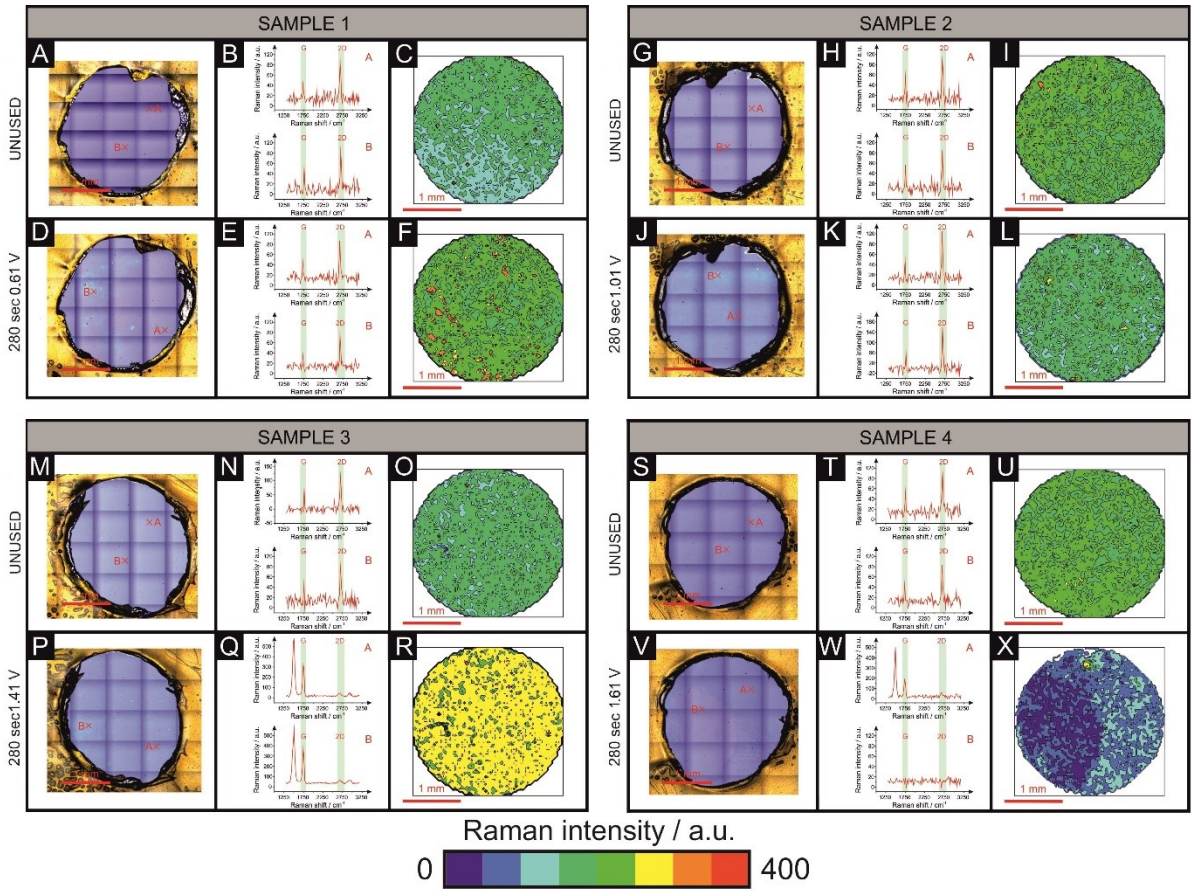

Figure 4. Chronoamperometry stability experiments using mono-layer graphene, holding a fixed potential at +0.61 V (A to F), +1.01 V (G to L), +1.41 V (M to R) and +1.61 V (S to X), showing optical images and Raman mapping characterisation before and after holding the fixed potential for 280 seconds. (Solution: 0.1 M KOH; *vs*. RHE). Raman maps show intensity of Graphene's G band (*ca*. 1590 cm^{-1}).

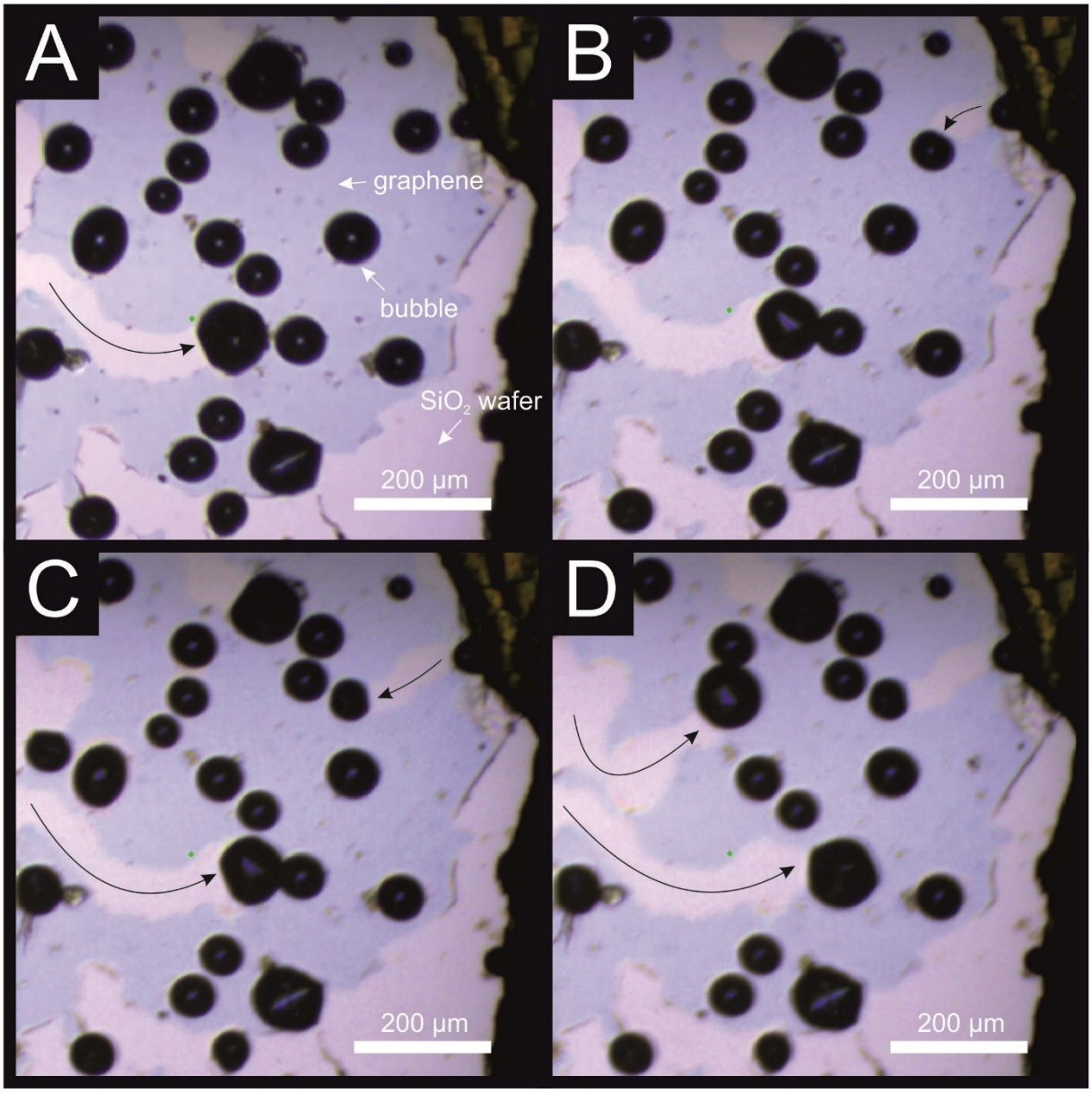

Figure 5. Screen-shot images captured/extracted from an *in-situ* experiment recorded while performing chronoamperometry (potential held a +1.61 V (*vs*. RHE)), using mono-layer graphene. Captions show the evolution of oxygen bubbles over the following time periods: 10 (A), 20 (B), 30 (C) and 40 (D) seconds. Black arrows indicate the movement of the bubbles damaging the surface of the electrode. (Solution: 0.1 M KOH).

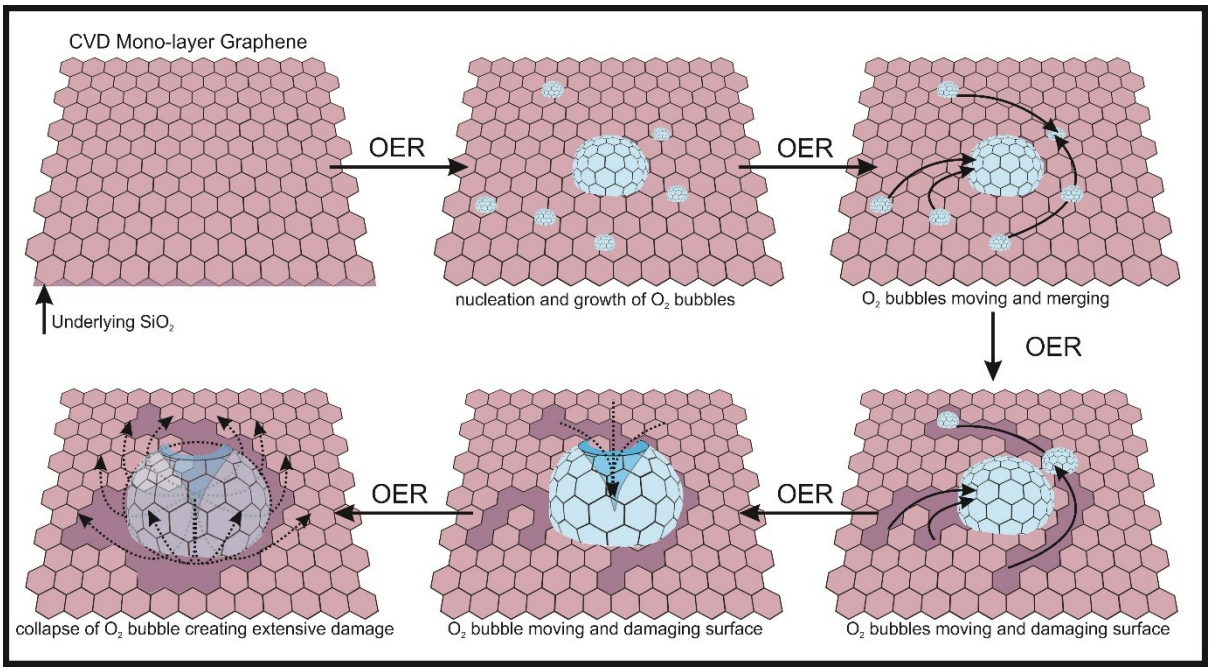

Figure 6. Schematic overview of oxygen bubbles growing (formed due to the OER) merging and collapsing, inducing structural damage to the surface of the mono-layer graphene electrode.

This work shows that a fixed potential of *ca*. +1.61 V (*vs.* RHE) oxidizes CVD graphene and induces the electrochemical oxygen evolution reaction (OER), generating oxygen bubbles that create a layer of defective mono-layer graphene (evidenced *via* Raman spectroscopy); more positive potentials induce higher levels of damage. Furthermore, linear sweep voltammetry (LSV) scans towards the OER show that faster scan rates cause extended and more critical structural damage. It is evident that mono-layer graphene is not a suitable electrode material for energy applications that require high positive potentials in alkaline media.

Graphene

Alejandro García-Miranda Ferrari, Dr. Dale A. C. Brownson, and Prof. Craig E. Banks*

Investigating the Integrity of Graphene towards the Electrochemical Oxygen Evolution Reaction (OER)

ToC figure: